Coupled Systems Mechanics, *Vol. 4, No. 4 (2015) 279-295*
DOI: http://dx.doi.org/10.12989/csm.2015.4.4.279

Modeling of the friction in the tool-workpiece system in diamond burnishing process

J.T. Maximov*, A.P. Anchev and G.V. Duncheva

Technical University of Gabrovo, Department of Applied Mechanicas, 5300 Gabrovo, Bulgaria

(Received April 11, 2015, Revised November 20, 2015, Accepted November 30, 2015)

Abstract. The article presents a theoretical-experimental approach developed for modeling the coefficient of sliding friction in the dynamic system tool-workpiece in slide diamond burnishing of low-alloy unhardened steels. The experimental setup, implemented on conventional lathe, includes a specially designed device, with a straight cantilever beam as body. The beam is simultaneously loaded by bending (from transverse slide friction force) and compression (from longitudinal burnishing force), which is a reason for geometrical nonlinearity. A method, based on the idea of separation of the variables (time and metric) before establishing the differential equation of motion, has been applied for dynamic modeling of the beam elastic curve. Between the longitudinal (burnishing force) and transverse (slide friction force) forces exists a correlation defined by Coulomb's law of sliding friction. On this basis, an analytical relationship between the beam deflection and the sought friction coefficient has been obtained. In order to measure the deflection of the beam, strain gauges connected in a "full bridge" type of circuit are used. A flexible adhesive is selected, which provides an opportunity for dynamic measurements through the constructed measuring system. The signal is proportional to the beam deflection and is fed to the analog input of USB DAQ board, from where the signal enters in a purposely created virtual instrument which is developed by means of Labview. The basic characteristic of the virtual instrument is the ability to record and visualize in a real time the measured deflection. The signal sampling frequency is chosen in accordance with Nyquist-Shannon sampling theorem. In order to obtain a regression model of the friction coefficient with the participation of the diamond burnishing process parameters, an experimental design with 55 experimental points is synthesized. A regression analysis and analysis of variance have been carried out. The influence of the factors on the friction coefficient is established using sections of the hyper-surface of the friction coefficient model with the hyper-planes.

Keywords: diamond burnishing; tool-workpiece system; slide friction coefficient; geometric nonlinearity; dynamic deflection; strain gage measurement

1. Introduction

It is well-known that the fatigue life of the metal engineering components is increased when in their surface layers, which are most loaded, beneficial residual normal compressive stresses are introduced through cold plastic deformation (Reid 1993, Su *et al*. 2008, Maximov *et al*. 2013). One of the methods by which low surface roughness, increased micro-hardness and residual

*Corresponding author, Professor, E-mail: maximov@tugab.bg

Copyright © 2015 Techno-Press, Ltd.
http://www.techno-press.org/?journal=csm&subpage=7 ISSN: 2234-2184 (Print), 2234-2192 (Online)

compressive stresses in the surface layers are achieved is slide diamond burnishing (Korzynski 2013, Korzynski *et al*. 2009, Korzynski *et al*. 2011). The essence of the method consists of elastic-plastic deformation of the surface layer as a result of compression of the deforming element to the workpiece under the influence of a normal elastic force, so that a sliding friction exists.

The increase of the slide friction coefficient leads to an intensive wear and the presence of adhesion of the metal particles on the diamond deforming element, and to a deterioration of the quality of the treated surface.

The friction coefficient in slide diamond burnishing includes two components – adhesion and deforming. The contribution of the first component constitutes (15÷40)% from the full friction coefficient (Yatzenko *et al.* 1985). According to Korzynski (2013) this coefficient is in the range 0.02÷0.08 when processing steels. Torbilo *et al*. (1976) state similar values for the friction coefficient (0.03÷0.08), and according to Yatzenko *et al*. (1985) the interval of change is 0.03÷0.12.

There are empirical relationships used to determine the deforming component of the friction coefficient in the case of small speeds. According to Yatzenko *et al*. (1985) this component depends on the radius of the spherical tip of the deforming diamond and on the depth of penetration in the workpiece, respectively on the burnishing force. The adhesion component does not depend on the process parameters and it is in the range 0.025÷0.05.

More extensive research on the friction coefficient in slide diamond burnishing process has been made in Russia at the end of 20th century (Hvorostuhin and Ilin 1973, Torbilo *et al*. 1976, Yatzenko *et al*. 1985). The study mainly deals with hard high-alloyed and high-carbon steels. The influence of different parameters on the friction coefficient is principally evaluated by the one-factor-at-the time method.

However, regression models for the friction coefficient with the participation of the four main process parameters (tool radius, burnishing force, feed rate, burnishing speed) are missing. Furthermore, information about the friction coefficient when processing rail steels R260 and 76 is also missing.

The dependence of the friction coefficient on the process parameters is important in two aspects:

- For finite element simulations of the diamond burnishing process (thermo-mechanical problem) in order to optimize the process parameters to achieve the desired quality of the treated surface layer (for instance residual stresses);
- For a multi-objective optimization of diamond burnishing process, since, by itself, the friction coefficient is an optimization criterion - with decreasing the coefficient, the quality of the processed surface increases. Furthermore, the combination of the friction coefficient, the burnishing force and the burnishing speed, results in power of the friction forces. This power is a measure of the generated heat, which (despite the presence of coolant), when above a certain limit, causes thermo-plastic deformation of the processed surface layer. These deformations change the distribution of the beneficial residual stresses in the treated surface layer in a negative direction.

In the present article a theoretical-experimental approach is developed for modeling the friction coefficient in diamond burnishing process of unhardened structural steels with a hardness of 220 HB. For this purpose a special device containing a beam with geometric nonlinearity is designed and manufactured. The dynamic deflection of this beam is correlated with the sought friction coefficient. This correlation is determined analytically (using the method of separation of the variables in the differential equation of the dynamic deflection of the elastic line) and is experimentally verified. The dynamic deflection in the experimental setup is measured

experimentally with a specially created virtual instrument in Labview. In order to obtain a regression model of the friction coefficient with the participation of the diamond burnishing process parameters, an experimental design with 55 experimental points has been synthesized. The influence of the factors on the friction coefficient is established using sections of the hyper-surface of the friction coefficient model with the hyper-planes.

2. A device for experimentally determining the friction coefficient

2.1 Basic idea

The geometrical nonlinearity of a deformable solid is expressed in a significant difference between the areas D and D_1 that the body occupies in the space, respectively in natural and elastic equilibriums. Because of that, the conditions for equilibrium are made for the deformed geometry. A particular case of geometrical nonlinearity of a straight beam, even at small displacements, is when the same is loaded simultaneously with an axial and a transverse force. For the two forces the principle of independence of their action is not applicable.

Such a beam structure with a geometrical nonlinearity is contained in the device developed by the authors for the experimental determination of the slide friction coefficient between the deforming element and the workpiece in the diamond burnishing process (Fig. 1). The burnishing force P_b is one of the main process parameters and the slide friction force T, transverse to the cantilever beam, is determined by Coulomb's law $T = \mu P_b$, where μ is the friction coefficient, which is to be determined. This coefficient depends on the manufacturing parameters of the diamond burnishing process: r - radius of the deforming diamond tip, P_b - burnishing force; f - burnishing feed; v - burnishing speed. It is assumed that Coulomb's law always holds true. Under the action of the two forces P_b and T, the elastic line of the beam is distorted and the deflection of the cross-section with abscissa $x = \xi$ is registered by an indicator. The force P_b is set by a helical spring with stiffness c, and the force T is determined by Coulomb's law. For specific pair P_b and μ, a corresponding deflection $w(\xi)$ is obtained. If the dependency $\mu = \mu[w(\xi)]$ is known, then for every measured $w(\xi)$ the friction coefficient will be readily calculated.

2.2 Physical model

Fig. 1 shows a photograph of the device (a), a scheme of work (b) and a beam model (c). An object of dynamic modeling is a cantilever beam with length L, constant cross-section, and bending stiffness EJ. The beam is loaded in its free end by transverse and axial forces and the ratio of their magnitudes is equal to μ (Fig. 1(c)). At the beam's free end mass m is concentrated. The traditional analytical method for dynamic analysis of beams is based on the well-known partial differential equation of the elastic line from fourth order concerning the metric coordinate and involving partial derivatives at the time from first and second orders, which account for the distributed resistance and inertial forces respectively. Very often in engineering applications the elastic line of the beam corresponds to its main semitone in free and forced

vibrations. For this reason in the present work the method developed by Maximov (2014) is used

• The function of the elastic line deflection is presented as

$$w(t,x)=\varphi(t)\,y(x) \tag{1}$$

where $\varphi(t)$ is a normal coordinate and $y(x)$ is a normal function (shape function of the elastic line);

• The normal function is selected in advance so as to satisfy the boundary conditions, using the trigonometric series method (Timoshenko 1922, Maximov 2014).

• Thus, the separation of the variables is carried out in advance, and the function of the normal coordinate is determined by solving an ordinary differential equation.

In this case (Fig. 1(c)), it is appropriate for the normal function to be chosen

$$y(x)=1-\cos\frac{\pi x}{2L} \tag{2}$$

where $x\in(0,L)$.

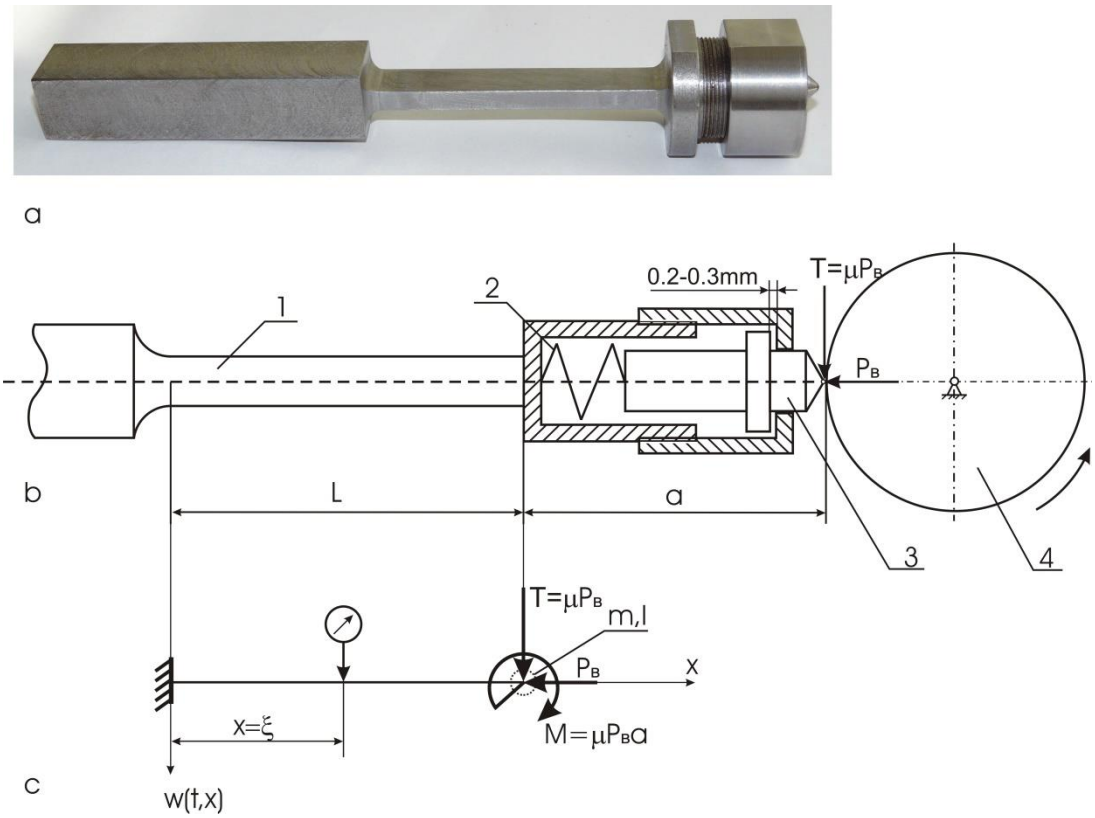

Fig. 1 Device and model: 1 - beam; 2 - spring; 3 - deforming element; 4 - workpiece

This function satisfies the boundary conditions: $y(0) = y'(0) = 0$.

Moreover, in the defined interval the curvature does not change its sign, i.e.:

$$y''(x) = \frac{\pi^2}{4L^2} cos \frac{\pi x}{2L} > 0 \quad \text{for} \quad \frac{\pi x}{2L} \in \left(0, \frac{\pi}{2}\right).$$

2.3 Dynamic behaviour

The equation of motion of the elastic line of the physical model of Fig. 1c is obtained from

$$\frac{d}{dt}\frac{\partial E_k}{\partial \dot{\varphi}} - \frac{\partial E_k}{\partial \varphi} + \frac{\partial E_p}{\partial \varphi} = Q_\varphi \tag{3}$$

The kinetic energy E_k is

$$E_k = E_k^b + E_k^m \tag{4}$$

where

$$E_k^b = \frac{\rho F}{2}\dot{\varphi}^2 \int_0^L y^2(x) dx = 0.1134 \rho F L \dot{\varphi}^2$$

is beam kinetic energy, ρ is density and $y(x)$ is defined by (2)

$$E_k^m = \frac{1}{2} m \dot{\varphi}^2 + \frac{1}{2}\frac{\pi^2}{4L^2} I \dot{\varphi}^2 \tag{5}$$

is kinetic energy of the concentrated mass, I is a mass moment of inertia about an axis defined by abscissa $x = L$ and perpendicular to the beam axis.

The beam potential energy is

$$E_p = \frac{EJ}{2}\varphi^2 \int_0^\ell [y''(x)]^2 dx = \frac{EJ\pi^4}{64L^3}\varphi^2 \tag{6}$$

Q_φ is the summarized force by the external load: transverse force $T = \mu P_b$ and axial force P_b (the forces of the weights of the beam and concentrated mass are ignored). The summarized force is determined by the principle of virtual displacements. An increase of the deflection w, equal to δw, is set which leads to a distortion of the elastic line

$$\delta w = \delta\varphi y(x) = \delta\varphi\left(1 - cos \frac{\pi x}{2L}\right)$$

and to the slope angle

$$\delta\left(\frac{\partial w}{\partial x}\right) = \delta\varphi y'(x) = \delta\varphi \frac{\pi}{2L} sin \frac{\pi x}{2L}.$$

The transverse force μP_b performs a virtual transverse displacement

$$\delta w_P = \delta\varphi\, y(x)\big|_{x=L} = \delta\varphi \tag{7}$$

The moment with magnitude $\mu P_b a$ performs a virtual rotation

$$\delta\varphi y'(x)\big|_{x=L} = \delta\varphi \frac{\pi}{2L} \tag{8}$$

The axial force P_b performs an axial displacement

$$\Delta L = \frac{1}{2}\int_0^L w'^2(x)dx = \varphi^2 \frac{\pi^2}{16L}$$

and the virtual axial displacement is

$$\frac{\partial \Delta L}{\partial \varphi}\delta\varphi = \frac{\pi^2}{8L}\varphi\delta\varphi \tag{9}$$

The virtual displacement of the summarized force Q_φ is $\delta\varphi$. Taking into account the relationships (7) - (9), from the equation of the virtual work

$$Q_\varphi \delta\varphi = \mu P_b \delta\varphi + \frac{\pi^2}{8L} P_b \varphi\delta\varphi + \frac{\pi a}{2L}\mu P_b \delta\varphi$$

the summarized force is determined

$$Q_\varphi = \mu P_b\left(1 + \frac{\pi a}{2L}\right) + \frac{\pi^2}{8L} P_b \varphi \tag{10}$$

In fact, the axial force P_b varies insignificantly in the process of diamond burnishing for two reasons:

- deviation from the correct geometric shape of the workpiece in cross-section and longitudinal section;
- machine spindle whipping.

The first reason has a stochastic nature of a particular workpiece and is not subject to an analytical model. The second reason leads to a change of burnishing force in accordance with a harmonic law with the frequency Ω of the machine spindle.

Let the machine spindle whipping is 2Δ. Then P_b can be presented as:

$$P_b = P_b^n + c\Delta \sin \Omega t$$

where c is the stiffness of the spring.

Changing the axial force magnitude from zero to P_b, due to the nature of the device from Fig. 1 shall be made for a time t_p, assuming a linear law. Then, for the axial force P_b, it follows

$$P_b = \frac{t}{t_p}\left(P_b^n + c\Delta \sin \Omega t\right) \text{ за } t \in (0, t_P) \tag{11}$$

$$P_b = P_b^n + c\Delta \sin \Omega t \text{ за } t \in (t_P, \infty) \tag{11a}$$

First, the dynamic behavior of the beam is considered in the time interval $t \in (0, t_P)$. From (3)-(6), (10) and (11) for the differential equation of change of the normal coordinate it follows

$$\ddot{\varphi} + \omega^2(t)\varphi = K_1 t + K_2 t \sin \Omega t \tag{12}$$

where

$$\omega(t) = \sqrt{\frac{EJ\pi^4}{32L^3 m^*} - \frac{\pi^2}{8Lm^*}\frac{t}{t_P}\left(P_b^n + c\Delta \sin \Omega t\right)} \tag{13}$$

$m^* = 0.2268\rho FL + m + \frac{\pi^2}{4L^2} I$ is the reduced mass, $K_1 = \mu\left(1 + \frac{\pi a}{2L}\right)\frac{P_b^n}{t_P m^*}$, $K_2 = \mu\left(1 + \frac{\pi a}{2L}\right)\frac{c\Delta}{t_P m^*}$.

The function $\omega(t)$ is visualized in Fig. 2 in the time interval $t \in (0, t_P)$ for the following numeric data: the beam cross-section is a rectangle $12 \times 6\ mm^2$, a length $L = 80mm$; $\rho = 7850\,kg/m^3$; $m = 0.05kg$; $I = 2 \times 10^{-5}\,kgm^2$; $a = 30mm$; $t_P = 1s$; $P_b^n = 400\,N$; $c = 10^5\,N/m$; $2\Delta = 0.05mm$; $\Omega = 40s^{-1}$. Due to the insignificant change of the function, it is accepted the same to be replaced by the constant

$$\omega = \sqrt{\frac{EJ\pi^4}{32L^3 m^*} - \frac{\pi^2 P_b^n}{8Lm^*}} \tag{14}$$

i.e., the frequency spectrum (13) is replaced by the eigenvalue (14) corresponding to the normal function (2).

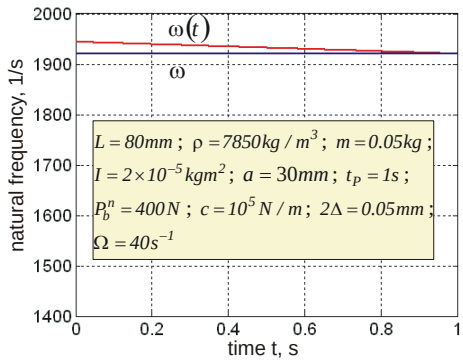

Fig. 2 Graph of the function $\omega = \omega(t)$

After substitution of (14) into (12), the total integral of the resulting equation with constant coefficients is

$$\varphi = c_1 \sin \omega t + c_2 \cos \omega t + \eta(t) \tag{15}$$

and the private integral $\eta(t)$ is sought by the method of undetermined coefficients in the form

$$\eta(t) = At + B + (Ct + D)\sin \Omega t + (Gt + H)\cos \Omega t \tag{16}$$

After substitution of (14) and (16) into (12) and equalizing the relevant coefficients, for unknown constants A, B, C, D, G and H it follows

$$A = \frac{K_1}{\omega^2};\ B = D = G = 0;\ C = \frac{K_2}{\omega^2 - \Omega^2};\ H = -\frac{2\Omega K_2}{\left(\omega^2 - \Omega^2\right)^2}.$$

The working frequency Ω always satisfies the condition $\Omega < \omega$, which can be seen from the graph and the numerical data in Fig. 2, since $\omega = 1920.5 s^{-1}$ and $\Omega = 10 \div 100 s^{-1}$.

The initial conditions are

$$\varphi(0) = \dot{\varphi}(0) = 0 \tag{17}$$

From (15)-(17) for the constants c_i it follows

$$c_1 = -\frac{K_1}{\omega^3};\ c_2 = \frac{2\Omega K_2}{\left(\omega^2 - \Omega^2\right)^2} \tag{18}$$

Finally, from (1), (2), (15), (16) and (18) for the functions of the dynamic deflection it follows

$$\begin{aligned} w(t,x) = \Bigg[& -\frac{K_1}{\omega^3}\sin \omega t + \frac{2\Omega K_2}{\left(\omega^2 - \Omega^2\right)^2}\cos \omega t + \\ & + \frac{K_1}{\omega^2}t + \frac{K_2}{\omega^2 - \Omega^2}t \sin \Omega t - \frac{2\Omega K_2}{\left(\omega^2 - \Omega^2\right)^2}\cos \Omega t \Bigg] \times \\ & \times \left(1 - \cos\frac{\pi x}{2L}\right) \end{aligned} \tag{19}$$

for $t \in (0, t_P)$, and

$$\begin{aligned} w(t,x) = \Bigg[& -\frac{K_1}{\omega^3}\sin \omega t + \frac{2\Omega K_2}{\left(\omega^2 - \Omega^2\right)^2}\cos \omega t + \\ & + \frac{K_1 t_P}{\omega^2} + \frac{K_2 t_P}{\omega^2 - \Omega^2}\sin \Omega t - \frac{2\Omega K_2}{\left(\omega^2 - \Omega^2\right)^2}\cos \Omega t \Bigg] \times \\ & \times \left(1 - \cos\frac{\pi x}{2L}\right) \end{aligned} \tag{20}$$

for $t \in (t_P, \infty)$.

2.4 Determination of the function $\mu = \mu[w(\xi)]$

Fig. 3 shows a visualization of (19) and (20) for $x = \xi = 60mm$. The amplitudes of the free vibrations (Fig. 3b) and of the forced vibrations (Fig. 3(c)) are respectively three and two orders smaller than the deflection (Fig. 3(a)) caused by the nominal magnitude of the burnishing force P_b in the interval $t \in (t_P, \infty)$. Moreover, in reality, the free vibrations are quickly hushed, mainly due to material hysteresis and energy dissipation at the place of the beam fixing. Therefore, with sufficient accuracy for the engineering practice, it can be worked with the static deflection, which is obtained when in (20) the harmonic functions are ignored

$$w(x) = \frac{K_1 t_p}{\omega_2}\left(1 - cos\frac{\pi x}{2L}\right)$$

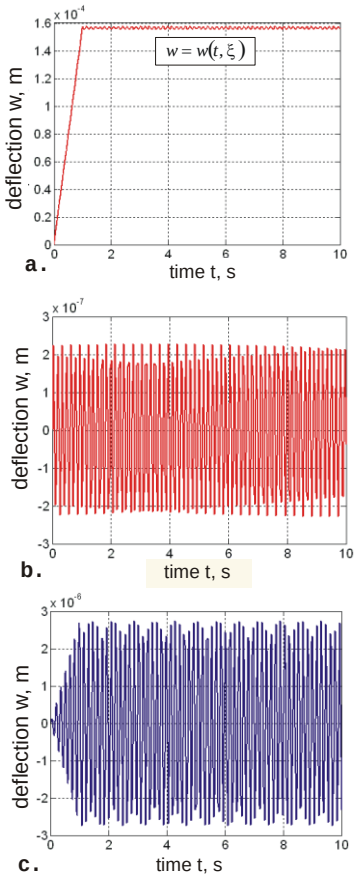

Fig. 3 Deflection of the section with abscissa $x = \xi = 60mm$ versus time: a. resultant deflection, (b) deflection by the free vibration with natural frequency, corresponding to the shape defined by (2) and (c) deflection by the free vibration

Taking into account (14) and the expression for K_1, the deflection of arbitrary section with abscissa $x=\xi$ takes the following form

$$w(\xi)=\frac{32\mu\left(1+\frac{\pi a}{2L}\right)P_b^n L^3}{EJ\pi^4-4\pi^2L^2P_b^n}\left(1-cos\frac{\pi\xi}{2L}\right) \tag{21}$$

For the desired function $\mu=\mu[w(\xi)]$ it follows

$$\mu=\varphi\left(P_b^n\right)w(\xi) \tag{22}$$

where

$$\varphi\left(P_b^n\right)=\frac{EJ\pi^4-4\pi^2L^2P_b^n}{32\left(1+\frac{\pi a}{2L}\right)P_b^n L^3\left(1-cos\frac{\pi\xi}{2L}\right)}\,. \tag{23}$$

The denominator of (21) is always greater than zero since

$$P_b^n << P_{b,cr}^n=\frac{EJ\pi^2}{(2L)^2},$$

where $P_{b,cr}^n$ is the known Euler's critical force for the first case of fixing

2.5 Experimental verification

An experimental verification is made of the dependence of the deflection by the transverse force T (see Fig. 1(b)). The analytical form of this dependence is obtained from (21) after substitution of $\mu P_b^n=T$

$$w(\xi)=kT \tag{24}$$

where

$$\kappa=\frac{32\left(1+\frac{\pi a}{2L}\right)L^3}{EJ\pi^4-4\pi^2L^2P_b^n}\left(1-cos\frac{\pi\xi}{2L}\right) \tag{25}$$

Obviously the imported by the burnishing force P_b^n geometric nonlinearity is negligible.

The experimental setup for experimental determination of the dependence $w(\xi)=f(T)$ is depicted in Fig. 5 and Fig. 6 shows the obtained experimental outcomes. The comparison for k is carried out for the case when $P_b^n=0$ - the value of the function $k\left(P_b^n\right)\Big|_{P_b^n=0}$ is reported by Fig. 4, since the experiment is conducted without the existence of an axial force P_b^n.

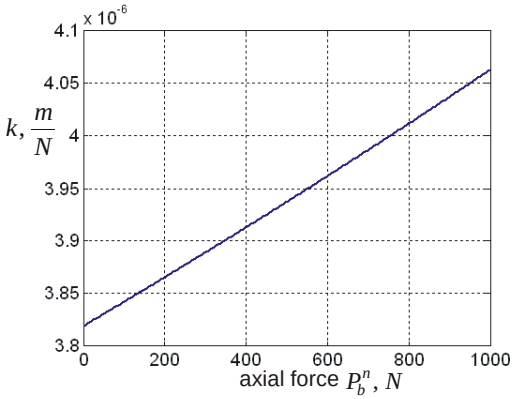

Fig. 4 Graph of the dependence $k = k\left(P_b^n\right)$

Fig. 5 Experimental determination of the dependence $w(\xi) = f(T)$

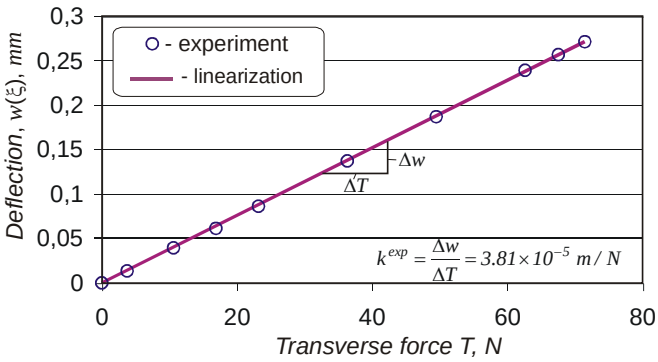

Fig. 6 Experimental results

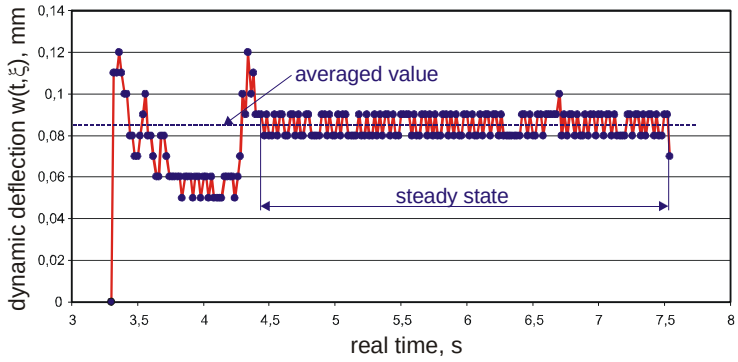

Fig. 7 Typical graphic of the experimentally obtained dependence $w = w(\xi, t)$

From Fig. 6 for the slope of the straight line $k^{exp} = 3.81 \times 10^{-6}\ m/N$ is obtained and from Fig. 4

$$k\left(P_b^n\right)\Big|_{P_b^n=0} = 3.825 \times 10^{-6}\, m/N$$

is accounted. The obtained result gives a basis for formula (25), respectively the graph in Fig. 4, to be considered credible and reliable, which means that formulas (22) and (23) for determining the friction coefficient are also credible and reliable.

3. Experiment study

3.1 Conditions of the experiment

● The objective function is the friction coefficient μ. The latter was calculated by (22), where the deflection $w(\xi)$ is experimentally determined for each point of the experimental plan and the component (23) is a function of the burnishing force F_b. The deflection $w(\xi)$ is an average value of the measured dynamic deflection $w(\xi, t)$, which is a function of time. Fig. 7 shows a typical graphic of the function $w(\xi, t)$ and its averaged value - in the case of point №9 from the experimental design.

● The governing factors are: radius r of the spherical tip of the deforming element, made of synthetic diamond; burnishing force P_b; burnishing feed rate f; burnishing feed v. The varying levels of the governing factors are shown in Table 1. The factors measured in natural physical units are marked with $\tilde{x}_i$. During the experiment each of the factors $\tilde{x}_i$ alters in a given interval $\tilde{x}_{i,min} \le \tilde{x}_i \le \tilde{x}_{i,max}$. The lower limit $\tilde{x}_{i,min}$ of this interval is called lower level, the upper one $\tilde{x}_{i,max}$ is upper level and the middle $\tilde{x}_{i,0}$ of this interval is the factor's basic level. The factors used in the experiment have different dimensions. In order to eliminate the experimental plan's dependence from the dimensions, the factors $\tilde{x}_i$ are transformed into a coded

form x_i through dependence

$$x_i = \left(\tilde{x}_i - \tilde{x}_{i,0}\right) / \left|\tilde{x}_{i,max} - \tilde{x}_{i,0}\right| \tag{26}$$

● The specimens material is an unhardened low-alloy constructional steel 37Cr4 with hardness of 220 HB. The carried out indentation test (about the nature of such a test see for example Sartkulvanich *et al*. 2007) showed that the behavior of the surface layer of this steel is similar to that of the rail steels R260 and 76. In this experiment steel 37Cr4 is used, since it is more prevalent in the form of rolled metal, which is suitable for producing axisymmetric samples. The latter have a diameter of 36 mm. The initial roughness of the samples is in the range $1.2 \div 2.4 \mu m$ under criterion Ra, according to recommendations given by Korzynski (2013).

● Synthetic deforming diamond with spherical tip is used. The experiment is carried out on a conventional lathe C11. A lubricant-cooler Hakuform 70-19 is used.

Table 1 Governing factors and their levels

		Levels of the factors		
		Coded (Dimensionless)		
Governing factors		-1	0	+1
Natural $\tilde{x}_i$	Coded x_i		Natural	
Diamond radius, $r\,[mm]$, $\tilde{x}_1$	x_1	1	3	5
Burnishing force, $F_b\,[N]$, $\tilde{x}_2$	x_2	100	300	500
Burnishing feed, $f\,[mm/rev]$, $\tilde{x}_3$	x_3	0.075	0.15	0.225
Burnishing speed, $v\,[m/min]$, $\tilde{x}_4$	x_4	80	110	140

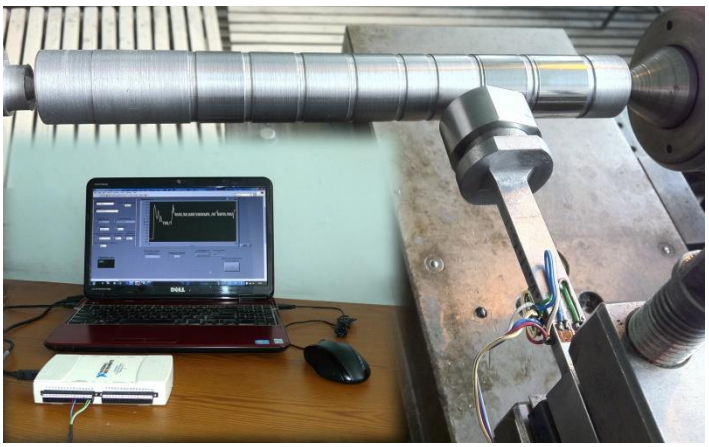

Fig. 8 Experimental setup

● The experimental setup is shown in Fig. 8. In order to measure the deflection of the beam, strain gauges connected in a “full bridge” type of circuit are used. The connected scheme does not account the compressive force in the beam and has the highest sensitivity regarding the bending moment. A flexible adhesive is selected, which provides an opportunity for dynamic measurements through the constructed measuring system. The signal is proportional to the beam deflection and is fed to the analog input of USB DAQ board, from where the signal enters in a purposely created virtual instrument which is developed using Labview. The basic characteristic of the virtual instrument is the ability to record and visualize the measured deflection in real time. The signal sampling frequency is 50 Hz, which is chosen in accordance with the theorem of sampling of signals (Nyquist-Shannon sampling theorem).

3.2 Experimental design

An optimal composed second-order design with 24 experimental points is expanded to 55 experimental points in order to conduct preliminary experiments using the one-factor-at-the time method with at least three experimental points. By means of QstatLab (Vuchkov and Vuchkov 2009) a regression analysis of the obtained experimental results is carried out. For the objective function (friction coefficient μ)

$$\mu = 0.0541 - 0.0426x_1 - 0.0087x_2 - 0.0109x_3 + 0.0041x_4 + 0.0319x_1^2 + 0.008x_2^2 + \\ + 0.0065x_4^2 + 0.0233x_1x_3 - 0.0078x_2x_3 \quad (27)$$

is obtained, where x_i is determined by the dependence (26).

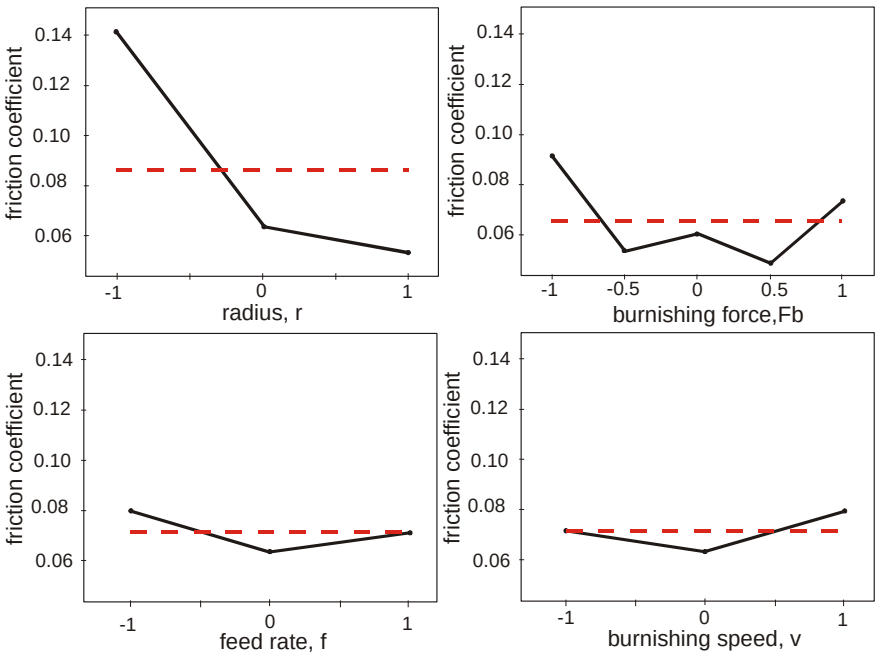

Fig. 9 Graphics of the main effects of the factors

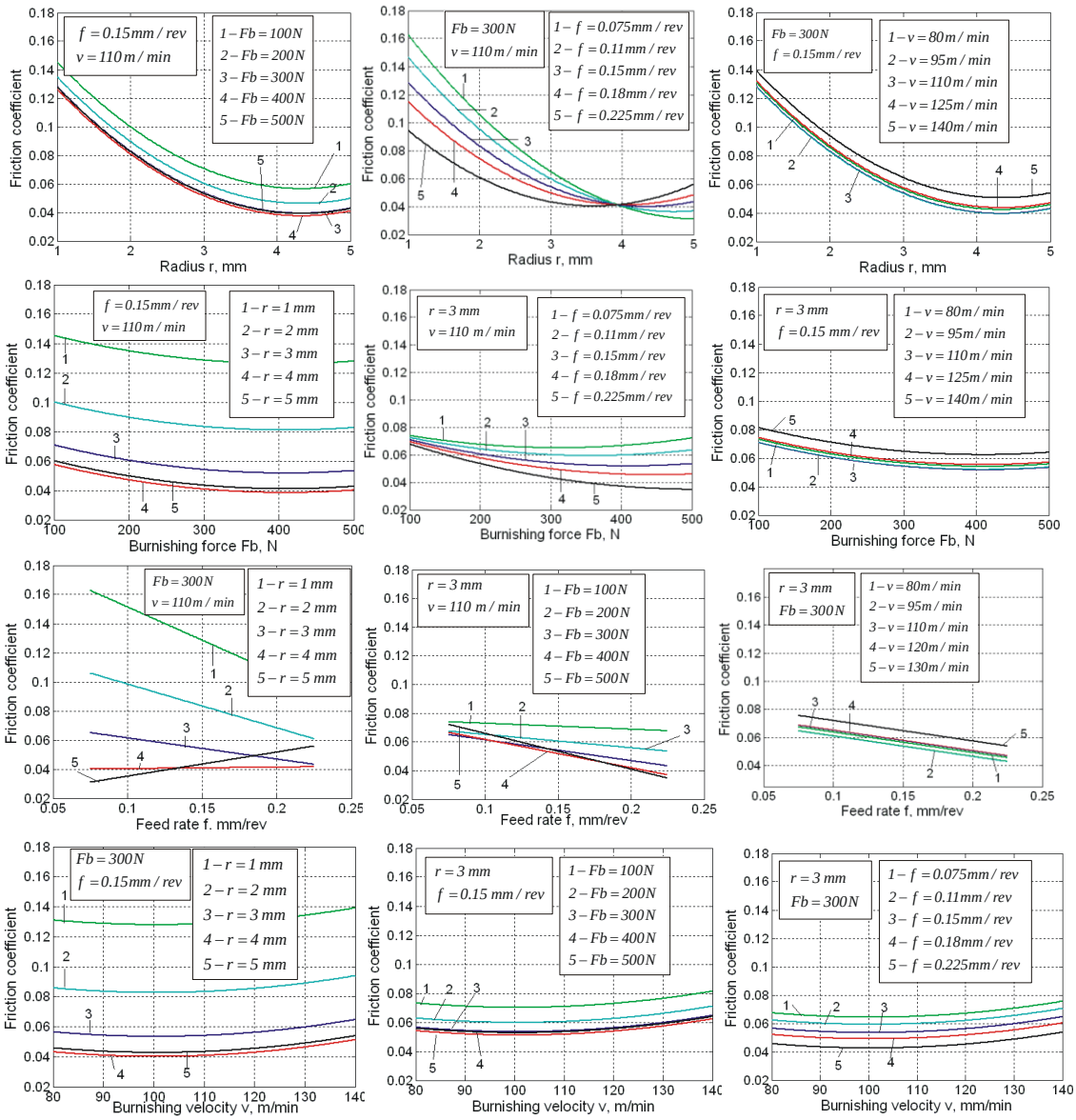

Fig. 10 Sections of the hyper-surfaces of the friction coefficient model with different hyper-planes

Eq. (27) has an empirical nature since it is obtained by an experimental way and a regression analysis on the basis of an experimental design. It is not obtained by analytical approach on the basis of physical laws.

In order to estimate the significance of the governing factors as well as the interaction between them, the factors are presented in coded mode (dimensionless) in the regression model in accordance with Eq. (26). Each factor is changed in the interval $-1 \le x_i \le 1$. Then the

coefficients in Eq. (27) have the dimension of the objective function, and the absolute values of these coefficients are a measure of the importance of the factors as well as the interaction between them. For instance, the interaction between the factors x_1 and x_3 is most greatly expressed.

Analysis of variance (ANOVA) has been conducted by means of QStatLab package in order to estimate in qualitative aspect the factors significance on the friction coefficient model. When the experimental approach for investigation of a given process is used, this is a generally accepted practice. The main effects of the factors have been shown in Fig. 9. Obviously, the most significant factor is the diamond radius x_1, and the feed rate x_3 has the least importance. In order to obtain the minimum values of the friction coefficient, it is necessary the diamond radius to be maximum and the remaining factors to have values around the middle of the range of variation of the corresponding parameter.

Fig. 10 shows sections of the hyper-surfaces of the friction coefficient model with different hyper-planes. From the four factors, of biggest influence on the friction coefficient has the radius of the diamond. Increasing of the radius from 1 to 5 mm, ceteris paribus, leads to a reduction of the friction coefficient by 4 times. From physical point of view this fact is expected since with increasing the radius, the depth of penetration of the diamond decreases, which leads to a reduction of both components, and hence of the overall friction coefficient. Fig. 10 confirms that the correlation between the diamond radius and the feed rate is most significant, as the trend is more pronounced for small feed rates.

4. Conclusions

A theoretical-experimental approach has been developed for modeling the coefficient of sliding friction in the dynamic system tool-workpiece in slide diamond burnishing of low-alloy unhardened steels. The designed experimental setup includes a nonlinear cantilever Bernoulli-Euler beam. An analytical relationship between the beam deflection and the sought friction coefficient has been obtained. From this relationship, after experimentally determining the beam deflection, the dependence of the friction coefficient on the diamond burnishing governing parameters has been obtained. The influence of the burnishing parameters on the friction coefficient has been established using sections of the hyper-surface of the friction coefficient model with the hyper-planes. It has been ascertained that the deforming diamond radius has the biggest influence and the feed rate has the smallest.

Acknowledgements

This work was supported by the Bulgarian Ministry of Education and Science and the Technical University of Gabrovo under Contract No M-1402. The authors express their special thanks to Eng. Velizar Kuzmanov for his help with the experiments.

References

Hvorostuhin, L.A. and Ilin, N.N. (1973), “Friction during diamond burnishing of metals and alloys”, *Vestnik mashinostroenie*, **11**, 64-65 (in Russian).

Korzynski, M., Lubas, J., Swirad, S. and Dudek, K. (2011), "Surface layer characteristics due to slide diamond burnishing with a cylindrical-ended tool", *J. Mater. Process. Tech.* , **211**(1), 84-94.

Korzynski, M., Pacana, A. and Cwanek, J. (2009), "Fatigue strength of chromium coated elements and possibility of its improvement with slide diamond burnishing", *Surf. Coat. Tech.*, **203**(12), 1670-1676.

Korzynsky, M. (2013), "Slide diamond burnishing", (Ed., Korzynski, M.), *Nonconventional Finishing Technologies*. Polish Scientific Publishers, Warsaw.

Maximov, J.T. (2014), "A new approach to modeling the dynamic response of Bernoulli-Euler beam under moving load", *Coupled Syst. Mech.*, **3**(3) 247-265.

Maximov, J.T., Duncheva, G.V. and Amudjev, I.M. (2013), "A novel method and tool which enhance the fatigue life of structural components with fastener holes", *Eng. Fail. Anal.*, **31**, 132-143.

Reid, L. (1993), "Beneficial residual stresses at bolt holes by cold expansion", (Eds., J.J. Kalker *et al*.), *Rail Quality and Maintenance for Modern Railway Operation*, Kluwer Academic Publishers, Printed in Netherlands.

Sartkulvanich, P., Altan, T., Jasso, F. and Rodriguez, C. (2007), "Finite element modeling of hard roller burnishing: an analysis on the effects of process parameters upon surface finish and residual stresses", *J. Manuf. Sci. Eng.*, **129**(4), 705-716.

Su, M., Amrouche, A., Mesmacque, G. and Benseddiq, N. (2008), "Numerical study of double cold expansion of the hole at crack tip and the influence on residual stress field", *Comput. Mater. Sci.*, **41**(3), 350-355

Timoshenko , S.P. (1972), *Theory of elasticity*, Naukova Dumka, Kiev (In Russian)

Torbilo, V.M., Evsin, E.A. and Chigodaev, N.E. (1976), "Friction of diamond element on steel", *Mashinovedenie*, **5**, 103-109 (in Russian).

Vuchkov, I.N. and Vuchkov, I.I. (2009), *QStatLab Professional, v. 5.5 – Statistical Quality Control Software*, User's Manual, Sofia,.

Yatzenko, V.K., Zaitzev, G.Z., Pritchenko, V.F. and Ivshtenko L.I. (1985), *Enhancement of load-carrying capacity of machine components by diamond burnishing*, Moscow: Machinostroenie (in Russian).